eMicrobe
https://www.sciltp.com/journals/emicrobe

Article

Glutathione Peroxidase from *Talaromyces marneffei* Interacts with Host Protein MOB1A: Insights from Molecular Dynamics Simulation

Yin Htet Htet Aung and Monsicha Pongpom *

Department of Microbiology, Faculty of Medicine, Chiang Mai University, Chiang Mai 50200, Thailand
* Correspondence: monsicha.p@cmu.ac.th

How To Cite: Aung, Y.H.H.; Pongpom, M. Glutathione Peroxidase from *Talaromyces marneffei* Interacts with Host Protein MOB1A: Insights from Molecular Dynamics Simulation. *eMicrobe* **2026**, *2*(3), 13. https://doi.org/10.53941/emicrobe.2026.100013

Received: 13 April 2026
Revised: 23 June 2026
Accepted: 22 July 2026
Published: 30 July 2026

Abstract: *Talaromyces marneffei* is an opportunistic intracellular fungal pathogen that survives within macrophages by adapting to oxidative stress. Glutathione peroxidase (TmGpx1) contributes to antioxidant defense; however, its potential role in host–pathogen interactions has never been investigated. In this study, a yeast two-hybrid assay identified several host partner proteins, including MOB1A (MOB Kinase Activator 1A), a scaffold protein in the Hippo signaling pathway. To support this interaction, computational molecular dynamics simulations were performed, and the predicted interface was benchmarked against the canonical NDR (nuclear Dbf2-related)–MOB1A complex. The TmGpx1–MOB1A complex formed a stable interaction throughout the simulation, as indicated by consistent minimum distances, contact numbers, hydrogen bonding, and buried surface areas. However, compared to the NDR–MOB1A complex, the TmGpx1 interaction exhibited fewer intermolecular contacts and hydrogen bonds, a smaller interfacial area, and weaker binding free energy, indicating a less optimized interaction. Molecular Mechanics/Poisson-Boltzmann Surface Area (MM/PBSA) analysis supported spontaneous binding for both complexes, with weaker binding for TmGpx1–MOB1A (ΔG, −56.18 ± 23.11 kcal/mol) compared with NDR–MOB1A (ΔG, −127.24 ± 35.60 kcal/mol). MOB1A maintained structural stability upon binding to TmGpx1. Although these results supported weaker MOB1A binding, the presence of TmGpx1 is meaningful and motivates future experimental testing of whether TmGpx1 can modulate host Hippo-pathway-associated signaling during *T. marneffei* infection.

Keywords: protein-protein interactions; glutathione peroxidase; MOB1A; moonlighting protein; Hippo signaling; MD simulation

1. Introduction

Talaromyces marneffei is an opportunistic fungal pathogen endemic to Southeast Asia [1]. It primarily causes disseminated infections in immunocompromised individuals, particularly those with HIV/AIDS [2]. Infection is initiated through inhalation of environmental conidia, which are subsequently engulfed by alveolar macrophages. Within macrophages, *T. marneffei* undergoes a morphological transition from the mold to the yeast form, enabling intracellular survival, replication, and disease progression [3].

The molecular mechanisms underlying adaptation and intracellular survival of *T. marneffei* are not fully understood. The host response to this fungus involves complex interactions, particularly within macrophages, where the pathogen must withstand intracellular defense mechanisms [4,5]. One of the primary antimicrobial strategies employed by macrophages is the production of reactive oxygen species (ROS) and reactive nitrogen

species (RNS) during the oxidative burst. To survive these conditions, fungal pathogens rely on antioxidant systems that mitigate oxidative damage and maintain redox homeostasis. Among these, the glutathione system plays a crucial role in protecting cells from oxidative stress [3]. Glutathione peroxidases are key enzymes within this system, catalyzing the reduction of hydrogen peroxide and organic hydroperoxides using glutathione as a reducing substrate. Furthermore, genes involved in glutathione metabolism are differentially expressed across developmental stages and are induced under oxidative stress conditions, highlighting their importance in fungal adaptation within host environments [3]. In addition to its role in oxidative stress defense, glutathione peroxidase in *T. marneffei* (TmGpx1) has been identified as an antigen capable of eliciting antibody responses in infected patients [6]. TmGpx1 is one of the proteins exported outside the cells through extracellular vesicles (EVs) [7,8]. As the EV is one of the virulence-associated structures in microorganisms, its excretion from the fungal pathogen and engulfment by host macrophages are highly associated with fungal pathogenicity. The role of the glutathione peroxidase enzyme in host modulation has not been investigated in *T. marneffei* infection.

Enzymes in the glutathione system have also been shown to contribute to host–pathogen interactions. For instance, the Ure2 protein in *S. cerevisiae*, which possesses glutathione S-transferase activity in addition to other functions, also participates in nitrogen catabolite repression [9]. There was evidence that several fungal proteins function as moonlighting proteins, performing multiple independent biological functions without gene fusion or alternative splicing [8,10]. Considering this discovery, our results from a yeast two-hybrid (Y2H) experiment utilizing TmGpx as bait indicated its ability to bind to several proteins within the cytoskeletal system, suggesting the moonlighting capability of TmGpx1 [11]. The Y2H assay identified several host-interacting proteins, for instance, an FK506-binding protein (FKBP), a protein associated with host cytoskeletal function. This study focused on one of the identified macrophage proteins, MOB1A. The interaction between TmGpx1 and MOB1A was investigated with a molecular dynamics (MD) simulation and benchmarked with a MOB1A canonical partner, NDR1.

MOB1A is a conserved scaffold protein in the Hippo signaling pathway and plays a central role in activating NDR and LATS (large tumor suppressor) family kinases [12]. MOB1A directly binds to NDR kinases and promotes their activation by relieving autoinhibitory conformations [13]. NDR kinases, members of the AGC (protein kinase A, G, and C) family of serine/threonine kinases, play important roles in regulating cytoskeletal organization and cell polarity [14,15]. Once activated, NDR kinases influence downstream signaling pathways, including the regulation of Rho-family GTPases such as Cdc42, which are critical for actin cytoskeleton remodeling. Through downstream effectors such as Pard3, the signaling axis contributes to the establishment of cell polarity and directional migration [16]. In macrophages, cytoskeletal remodeling is essential for processes such as phagocytosis, migration, and immune surveillance. Therefore, disruption or modulation of the MOB1A–NDR signaling axis has the potential to alter macrophage behavior during infection. Given the central role of MOB1A as a scaffold protein in kinase activation and cytoskeletal regulation, interactions between microbial proteins and MOB1A may represent a potential mechanism by which pathogens affect the function of host cells. Recent studies have demonstrated that the bacterial pathogen *Legionella pneumophila* could exploit the host Hippo pathway to promote infection and intracellular survival [17].

Based on this rationale, we hypothesize that TmGpx1 may interact with MOB1A in the host macrophage, modulate the signaling pathways, and support the pathogenesis of *T. marneffei*. Because Y2H does not define the binding mode or stability of the host-pathogen protein partners, we applied MD analysis in this study. We evaluated stability using root-mean-square deviation (RMSD) and root-mean-square fluctuation (RMSF), interfacial contacts and hydrogen bonds, buried surface area, and binding energetics (MM/PBSA) and compared these metrics with the NDR–MOB1A reference complex.

2. Materials and Methods

2.1. Yeast Two-Hybrid (Y2H) Assay

ULTImate Y2H analysis was performed by Hybrigenics Services (Hybrigenics Services, Paris, France, http://www.hybrigenics-services.com/; accessed on 11 December 2024). The coding sequence of the bait protein TmGpx1 (PMAA_007230, Hyr1, 197 amino acids) from *Talaromyces marneffei* ATCC18224 was synthesized and cloned in-frame to generate the pB27, N-LexA-bait-C fusion vector. The resulting LexA–TmGpx1 fusion construct was used to screen for interacting proteins by mating with yeast cells harboring a randomly primed, non-induced human macrophage cDNA library (Macrophage_RP1, prey). Following mating, positive interactions were selected, and prey fragments from positive clones were PCR-amplified, sequenced, and identified through comparison with the NCBI GenBank database using BLAST analysis. The Predicted Biological Score (PBS) was calculated to evaluate the confidence of each identified protein–protein interaction. A PBS was assigned, ranging from category A (highest confidence) to category E (lowest confidence), based on statistical analysis of prey

fragment occurrence and the background interaction probability. Interaction domains of the prey proteins were analyzed using DomSight, which maps the minimal Selected Interaction Domain (SID) of prey proteins alongside known functional and structural motifs, enabling the identification of potential binding regions within each interacting partner.

2.2. Protein Modeling

Protein sequences for each protein (Gpx1, MOB1A, NDR) were obtained from NCBI to predict the protein complex structure and used as input for https://alphafoldserver.com (accessed on 12 February 2026) [18], and a 3D structural model was computationally generated. Among the five models retrieved from the program, the best model was selected based on the ranking scores, using pTM (predicted template modeling) and ipTM (interface predicted template modeling), and was subsequently used for MD simulation. The confidence scores of the selected models, including pTM, ipTM, and ranking scores, are reported in Table S1. The TmGpx1–MOB1A complex exhibited moderate overall confidence (pTM = 0.70) and moderate interface confidence (ipTM = 0.57), whereas the NDR–MOB1A complex showed moderate overall confidence (pTM = 0.61) but high interface confidence (ipTM = 0.81).

2.3. Molecular Dynamics (MD) Simulation

Molecular dynamics (MD) simulations were performed on an HPE Apollo 6500 high-performance computing system (Hewlett Packard Enterprise, Spring, TX, USA) equipped with AMD EPYC 7742 processors and NVIDIA A100 SXM4 GPUs. All simulations were performed using the GROMACS software package (version 2022.4) [19].

Initial protein structures generated by AlphaFold3 were converted into GROMACS-compatible topology files using the gmx pdb2gmx module, with the AMBER99SB force field applied. Each protein–protein complex was subsequently placed at the center of a cubic simulation box with 1.0 nm between the solute and the box boundaries to avoid artificial interactions. The system was solvated using the three-point TIP3P water model [20].

To reproduce physiological conditions, counterions were added to neutralize the system, and additional sodium and chloride ions were introduced to achieve a final salt concentration of 0.15 M. Ion placement was performed using the gmx genion tool following system preprocessing with gmx grompp.

Energy minimization was conducted using the steepest descent algorithm to eliminate steric clashes and optimize the system geometry. This was followed by a two-phase equilibration procedure consisting of constant volume and temperature (NVT) and constant pressure and temperature (NPT) ensembles, each performed for 100 ps.

Production MD simulations were then carried out for 200 ns per replicate for triplicates using the leapfrog integrator with a 2 fs time step. Trajectory coordinates were saved every 10 ps for downstream analysis. Hydrogen-containing bonds were constrained using the LINCS algorithm. The Verlet cutoff scheme was used for neighbor searching. Short-range van der Waals and electrostatic cutoffs were both set to 1.2 nm, with force-switching applied to van der Waals interactions from 1.0 to 1.2 nm. Long-range electrostatics were treated using the particle mesh Ewald method. Temperature was maintained at 298 K using the V-rescale thermostat with a coupling time constant of 1.0 ps. Pressure was maintained at 1.0 bar using isotropic C-rescale pressure coupling with a coupling time constant of 5.0 ps. Periodic boundary conditions were applied in all directions.

For trajectory analysis, simulation output files were concatenated using gmx trjcat, and periodic boundary conditions were corrected by centering the system using gmx trjconv. The structural dynamics of the protein complex were assessed by RMSF (Root Mean Square Fluctuation). The binding interface between interacting proteins was further assessed by determining the buried surface area (BSA), providing insights into the extent of intermolecular contact. The stability of the interaction was also examined by measuring the minimum distance between the two proteins over time using gmx mindist. In addition, intermolecular contacts were quantified by calculating the number of atomic contacts between the interacting partners throughout the simulation.

Hydrogen bonding interactions at the protein–protein interface were analyzed using the gmx hbond module, which determines both the presence and number of hydrogen bonds throughout the simulation. All analyses were performed across six independent replicate simulations (three for the reference pair and three for the test pair) to ensure consistency and reproducibility of the observed interaction patterns.

2.4. Per-Residue Decomposition Analysis Using gmx_MMPBSA

To quantify the contribution of individual amino acid residues to the binding free energy of the protein–protein complex, per-residue energy decomposition analysis was performed using the gmx_MMPBSA package [21]. The decomposition calculations were performed by generating the appropriate input parameters with the command gmx_MMPBSA --create_input gb pb decomp (idecomp = 1), following the recommended procedures described in the package documentation.

This approach enabled the partitioning of the total binding free energy into residue-wise contributions, thereby facilitating the identification of key residues at the interactive interface. The resulting energy components were analyzed using the gmx_MMPBSA_ana module, which provides both tabulated outputs and graphical representations of residue-level energy contributions.

Further data processing and visualization were performed using Microsoft Excel and Prism for graphical plotting. Three-dimensional structural representations of key interacting residues were generated using *PYMOL* to support the interpretation of interaction patterns.

3. Results

3.1. Yeast Two-Hybrid Screening

To identify the host proteins that interact with TmGpx1, a yeast two-hybrid (Y2H) assay was performed using TmGpx1 as bait against a human macrophage cDNA library derived from non-induced macrophages [11]. The screening analyzed approximately 73.5 million interactions, yielding 258 processed clones, and in total, sixteen candidate host proteins were identified, including the FK506-binding protein (FKBP) previously described in our related study [11]. MOB1A (Mps One Binder kinase activator 1A) was identified as one of the potentially interacting partners. Notably, MOB1A is a key adaptor protein in the Hippo signaling pathway, known to regulate kinase activation and cellular signaling dynamics [12]. Therefore, the identification of MOB1A in this assay revealed a potential interaction between TmGpx1 and host signaling machinery. Further analysis of prey fragments demonstrated that the MOB1A interacting domains correspond to structurally and functionally relevant regions of its signaling partner, NDR, supporting the biological plausibility of the detected interactions.

3.2. Characterization of Interactive Interface of TmGpx1–MOB1A and NDR–MOB1A Complexes

Molecular dynamics (MD) simulations were performed to determine the interaction between TmGpx1 and MOB1A over a 200 ns production simulation under physiological conditions. In this analysis, structural models of the NDR–MOB1A complexes were used as a reference for a canonical MOB1A-binding partner. The TmGpx1 and MOB1A appeared to form a complex within the early stage of the simulation, and this complex was stable until reaching the 200 ns analyzed time frame (Supplementary Figure S1). Backbone RMSD analysis was used to assess global structural stability of the complexes and individual components across three independent replicates per complex (six trajectories in total). The RMSD profiles for the full complexes and component proteins are shown in Supplementary Figure S2.

Structural characterization of the analyzed complexes obtained at 200 ns from the molecular dynamics simulations was subjected to *PyMOL* visualization. As shown in Figure 1, both complexes exhibit stable protein–protein associations, with MOB1A forming a well-defined interaction interface with its respective binding partner (Figure 1A,C). In the TmGpx1–MOB1A complex, representative interfacial contacts at 200 ns are illustrated by TmGpx1 residues 55 and 59 in proximity to MOB1A residues 131 and 149 (Figure 1B). Similarly, in the NDR–MOB1A complex, selected residue pairs, including NDR residues 55 and 136 and MOB1A residues 77 and 78, are shown to depict the interaction interface (Figure 1D). These residues were chosen as representative examples to visualize the binding interface and do not encompass all intermolecular contacts within each complex.

Together, these results demonstrated that TmGpx1 can form a structurally stable complex with MOB1A, engaging a binding surface similar to that of the canonical NDR partner, despite differences in local interaction geometry.

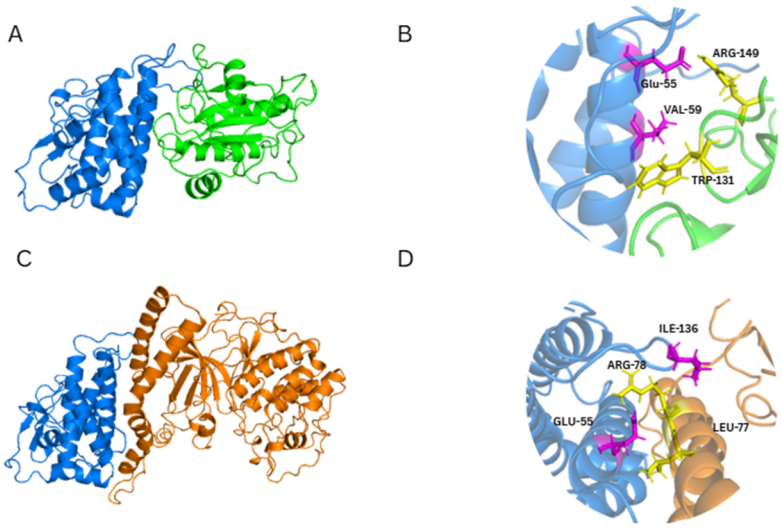

Figure 1. Structural overview of protein–protein complexes. (**A**) Overall structure of the TmGpx1–MOB1A complex. (**B**) Close-up view of the TmGpx1–MOB1A interface, highlighting key interacting residues, where TmGpx1 residues 55 and 59 are positioned in proximity to MOB1A residues 131 and 149, indicating a localized interaction region. (**C**) Overall structure of the NDR–MOB1A complex. (**D**) Close-up view of the NDR–MOB1A interface showing key contacts between NDR residues 55 and 136 and MOB1A residues 77 and 78, forming a defined binding surface. TmGpx1, MOB1A, and NDR molecules are presented in blue, green, and orange, respectively.

3.3. Interaction Stability and Characteristics

To evaluate the stability and interaction characteristics of the protein–protein complexes, minimum distance, intermolecular contacts, and hydrogen bonding were analyzed throughout the simulations (Figure 2).

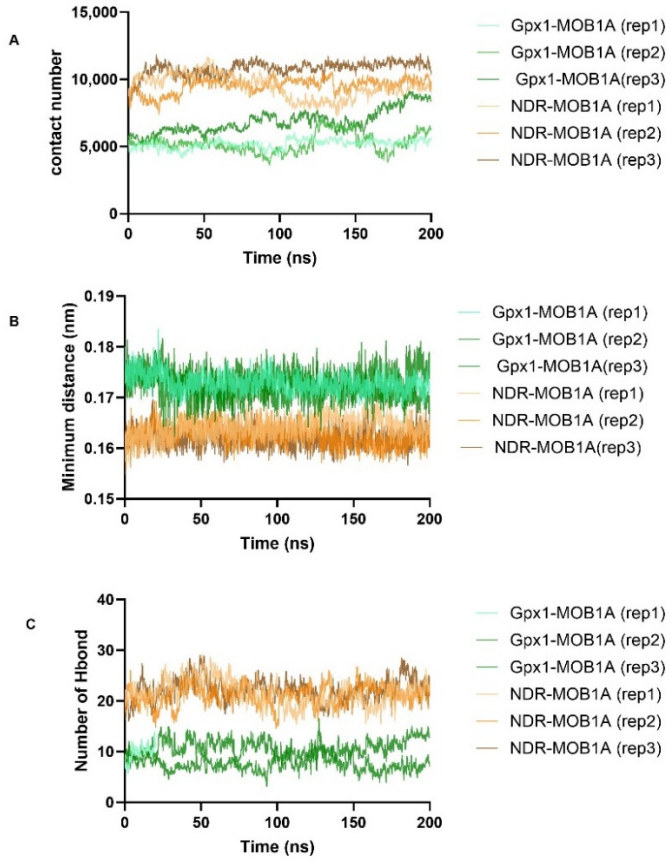

Figure 2. Interaction dynamics of protein–protein complexes during MD simulations. (**A**) Number of atomic contacts formed between the interacting proteins throughout the simulation, reflecting the extent of intermolecular interactions. (**B**) Minimum distance between protein partners over time, indicating the proximity and stability of

the interaction interface. (**C**) The number of hydrogen bonds formed between protein partners over time represents the stability and specificity of the interaction.

The minimum distance between the interacting partners remained consistently low in both systems, indicating stable complex formation (Figure 2B). The NDR–MOB1A complex exhibited a slightly lower average minimum distance (0.1629 ± 0.0010 nm) compared to the TmGpx1–MOB1A complex (0.1727 ± 0.0005 nm), suggesting a more compact interaction in the canonical complex. Importantly, no large fluctuations or separation events were observed in either system. These results showed that both systems remain consistently close, which proves that neither complex fell apart during the simulation.

Analysis of intermolecular contacts revealed a substantial difference in the interface boundary between the two complexes (Figure 2A). The NDR-MOB1A complex formed a significantly higher number of contacts (9939 ± 755 contacts) compared to the TmGpx1–MOB1A complex (5772 ± 951 contacts), meaning the NDR interface is much more crowded and extensive. Nevertheless, contact numbers in the TmGpx1 system remained stable across replicates, supporting the persistence of the interaction. Similarly, hydrogen bond analysis demonstrated that the NDR–MOB1A complex formed a greater number of intermolecular hydrogen bonds (21.68 ± 0.56 bonds) compared to the TmGpx1–MOB1A complex (9.42 ± 1.75 bonds) (Table 1, Figure 2C). These results indicate that NDR has significantly more stability than TmGpx1. Despite the reduced number of hydrogen bonds, the TmGpx1–MOB1A interaction maintained consistent hydrogen bonding throughout the simulation.

Together, these results demonstrated that both systems form stable protein–protein interactions; however, the NDR–MOB1A complex exhibits a more extensive and tightly packed interaction network. In contrast, the TmGpx1–MOB1A complex forms a less extensive but consistently maintained interface, supporting the formation of a stable yet weaker interaction.

Table 1. Comparison of interaction metrics (H-bonds, minimum distance, and contact number) between NDR–MOB1A and TmGpx1–MOB1A complexes.

	H Bond **Mean ± SD**	**Minimum Distance (nm)** **Mean ± SD**	**Contact Number** **Mean ± SD**
NDR-MOB1A Rep 1	21.66 ± 2.989	0.164 ± 0.00579	9468 ± 907.4
NDR-MOB1A Rep 2	21.14 ± 2.643	0.1625 ± 0.00577	9538 ± 593.7
NDR-MOB1A Rep 3	22.25 ± 2.752	0.1621 ± 0.005789	10,810 ± 594.4
Average NDR-MOB1A	21.68 ± 0.56	0.1629 ± 0.001	9939 ± 755
Gpx1-MOB1A Rep 1	9.851 ± 2.07	0.1729 ± 0.0056	5182 ± 381.2
Gpx1-MOB1A Rep 2	7.504 ± 1.8	0.173 ± 0.00674	5266 ± 711.8
Gpx1-MOB1A Rep 3	10.91 ± 2.054	0.1721 ± 0.005966	6869 ± 905.5
Average Gpx1-MOB1A	9.42 ± 1.75	0.1727 ± 0.0005	5772 ± 951

3.4. Structural Stability and Flexibility of the Protein Complex

To assess the impact of binding on receptor flexibility, root-mean-square fluctuation (RMSF) analysis was performed specifically for MOB1A in both complexes (Figure 3A,B). RMSF measures the average positional deviation of each residue over time, providing insight into local flexibility and structural stability. Overall, MOB1A exhibited similar fluctuation patterns in both the TmGpx1–MOB1A and NDR–MOB1A complexes, with most residues showing relatively low RMSF values. Regions of higher fluctuation were primarily confined to specific residue segments, likely corresponding to flexible loop or solvent-exposed regions. Importantly, no substantial increase in residue mobility was observed in the TmGpx1–MOB1A system compared to the NDR–MOB1A reference complex. This result supported that the global structure of MOB1A remains stable upon binding to either partner.

To quantify the extent of the protein–protein interaction interface, BSA was calculated throughout the 200 ns trajectory (Figure 3C). BSA represents the surface area that becomes inaccessible to solvent upon complex formation and is calculated as the difference between the solvent-accessible surface area (SASA) of the individual proteins and that of the protein complex. Therefore, higher BSA values indicate a larger interaction interface and stronger physical association between binding partners. The NDR–MOB1A complex exhibited a significantly higher BSA (39.42 ± 2.84 nm^2) compared to the TmGpx1–MOB1A complex (24.39 ± 3.54 nm^2), indicating that the canonical interaction forms a more extensive binding interface. This observation is consistent with the higher number of intermolecular contacts and hydrogen bonds identified in the NDR–MOB1A system. Despite having a smaller interface, the BSA values for the TmGpx1–MOB1A complex remained stable across three replicates, suggesting that the interaction interface is consistently maintained throughout the simulation. This result revealed

that while TmGpx1 forms a less extensive binding surface with MOB1A, the interaction is structurally stable and persistent over time.

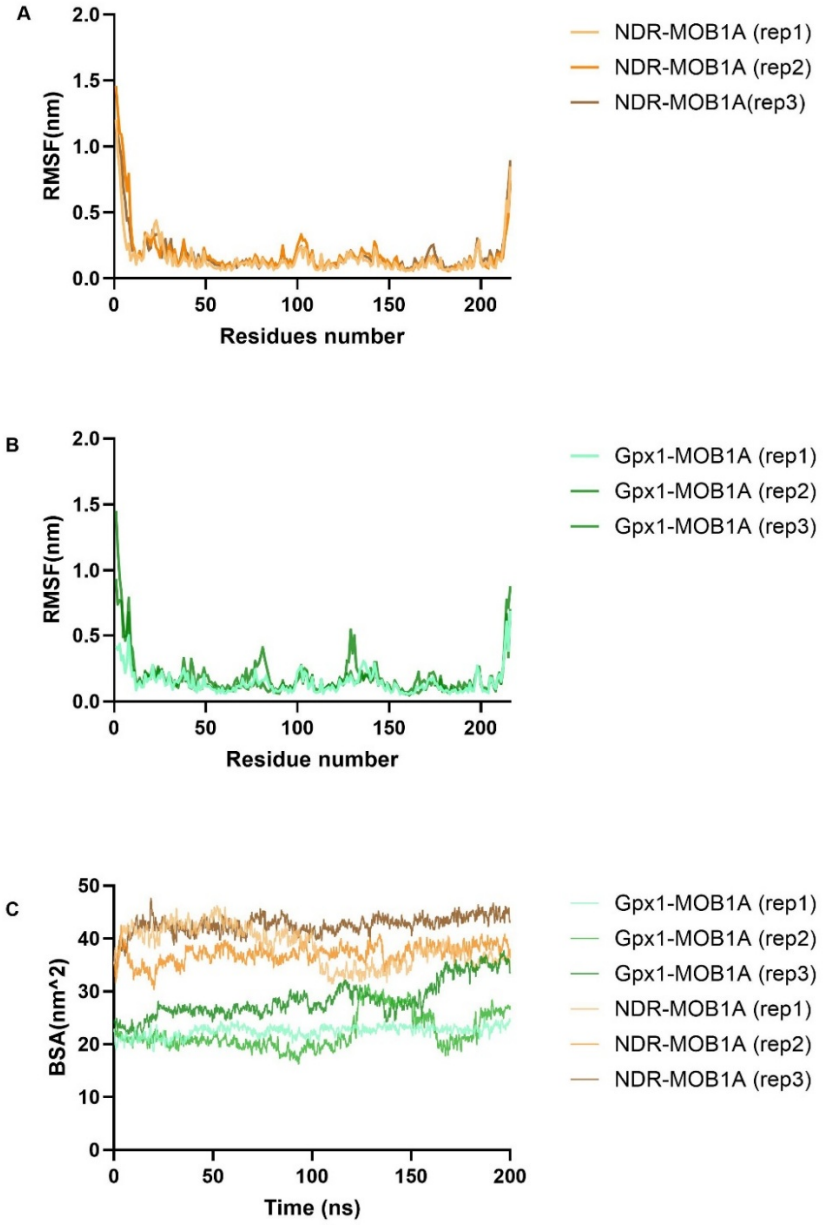

Figure 3. Structural stability and residue flexibility of protein–protein complexes. (**A**) RMSF profile of MOB1A residues in the NDR–MOB1A complex, indicating differences in flexibility of the receptor when bound to its native partner compared to TmGpx1. (**B**) Root mean square fluctuation (RMSF) profile of MOB1A residues in the TmGpx1–MOB1A complex, showing residue-level flexibility across the simulation. (**C**) Buried surface area (BSA) of NDR–MOB1A and TmGpx1–MOB1A complexes over the 200 ns course of the simulation, reflecting the extent of interface formation and stability.

These findings suggest that binding TmGpx1 does not induce significant structural destabilization of MOB1A. Instead, MOB1A maintains its structural integrity in both systems, supporting the formation of a stable complex regardless of the binding partner.

To quantitatively compare interface similarity between the TmGpx1–MOB1A and NDR–MOB1A complexes, we calculated contact overlap using the Jaccard similarity index across simulation replicates. The mean Jaccard similarity was 0.463 ± 0.046 (computed across nine pairwise replicate comparisons) (Table 2), indicating partial overlap between the two interfaces. These results support that TmGpx1 engages a partially overlapping but distinct MOB1A-binding mode compared with the canonical NDR–MOB1A complex.

Table 2. Interface contact overlap between TmGpx1–MOB1A and NDR–MOB1A complexes across replicate comparisons.

Comparison	Shared Residues	Union Residues	Jaccard
GPx1 rep1 vs. NDR rep1	56	113	0.496
GPx1 rep1 vs. NDR rep2	62	126	0.492
GPx1 rep1 vs. NDR rep3	61	116	0.526
GPx1 rep2 vs. NDR rep1	52	139	0.374
GPx1 rep2 vs. NDR rep2	66	144	0.458
GPx1 rep2 vs. NDR rep3	58	141	0.411
GPx1 rep3 vs. NDR rep1	53	116	0.457
GPx1 rep3 vs. NDR rep2	60	128	0.469
GPx1 rep3 vs. NDR rep3	58	119	0.487

3.5. Protein-Protein Binding Free Energy Analysis

3.5.1. Total Binding Affinity and Spontaneity

Total binding free energies (ΔTOTAL) for both the NDR–MOB1A (−140.2 ± 33.52 kcal/mol) and TmGpx1–MOB1A (−55.72 ± 16.36 kcal/mol) complexes exhibit negative values (Table 3). This result confirmed that both interactions are spontaneous and energetically favorable. However, the magnitude of binding for the NDR complex is significantly greater. This disparity reflects the superior energetic stability of the canonical interaction.

Although both complexes demonstrated negative binding energies, confirming spontaneous and energetically favorable interactions, the magnitude of binding was markedly reduced in the TmGpx1–MOB1A system. This difference reflects weaker overall intermolecular interactions, consistent with the reduced number of contacts, hydrogen bonds, and smaller buried surface area observed in Figures 2 and 3.

Table 3. Binding free energy decomposition of NDR–MOB1A and TmGpx1–MOB1A complexes calculated using the MM/PBSA method.

Component (kcal/mol)	NDR-MOB1A Rep1	NDR-MOB1A Rep2	NDR-MOB1A Rep3	NDR–MOB1A (Mean ± SD)	TmGpx1-MOB1A Rep1	TmGpx1-MOB1A Rep2	TmGpx1-MOB1A Rep3	TmGpx1–MOB1A (Mean ± SD)
ΔVDW	−160.39	−107.12	−184.12	−150.54 ± 39.43	−99.50	−62.87	−78.0	−80.12 ± 18.41
ΔEEL	−1120.74	−700.32	−1054.68	−958.58 ± 226.09	−664.85	−432.68	−448.77	−515.43 ± 129.65
ΔEGB	1154.23	721.44	1101.55	992.41 ± 236.14	705.75	464.35	483.56	551.22 ± 134.17
ΔESURF	−25.51	−16.07	−28.33	−23.30 ± 6.42	−13.93	−8.63	−10.8	−11.12 ± 2.66
ΔGGAS	−1281.13	−807.44	−1238.79	−1109.12 ± 262.12	−764.35	−495.55	−527.57	−595.82 ± 146.82
ΔGSOLV	1128.72	705.37	1073.21	969.10 ± 230.08	691.82	455.72	472.76	540.10 ± 131.67
ΔTOTAL	−152.41	−102.06	−165.58	−140.02 ± 33.52	−72.52	−39.83	−54.81	−55.72 ± 16.36

Energy components include van der Waals (ΔVDW), electrostatic (ΔEEL), polar solvation (ΔEGB), nonpolar solvation (ΔESURF), gas-phase energy (ΔGGAS), solvation energy (ΔGSOLV), and total binding free energy (ΔTOTAL). Values are presented as mean ± standard deviation from three independent simulations.

3.5.2. Drivers of Interaction and the Desolvation Penalty

In both interaction partners, the binding is primarily driven by van der Waals (ΔVDW) and electrostatic forces (ΔEEL), which together constitute the gas-phase interaction energy (ΔGGAS). Analysis results showed that the native NDR complex is more optimized (Table 3).

NDR exhibited substantially stronger electrostatic contributions (−958.58 ± 226.09 kcal/mol) compared to TmGpx1 (−515.43 ± 129.65 kcal/mol). Additionally, NDR similarly outperforms TmGpx1 in surface-to-surface interactions through van der Waals bonds (−150.54 ± 39.43 kcal/mol vs. −80.12 ± 18.41 kcal/mol). Moreover, these favorable interactions were partially offset by polar solvation energy (ΔEGB), which contributed positively (unfavorable) in both systems, reflecting the energetic penalty associated with desolvation during binding. This effect was more pronounced in the NDR–MOB1A complex (992.42 ± 236.14 kcal/mol) compared to TmGpx1–MOB1A (551.22 ± 134.17 kcal/mol). The non-polar solvation energy (ΔESURF) contributed favorably but to a lesser extent in both systems.

These results indicated that although similar types of interactions stabilize both complexes, the strength of these interactions is significantly greater in the NDR–MOB1A system.

3.5.3. Conserved Hotspots vs. Reduced Energetic Optimization

Per-residue energy decomposition determined by MM/PBSA calculations (Figure 4A) revealed that TmGpx1 and NDR engage the same functional interface on MOB1A.

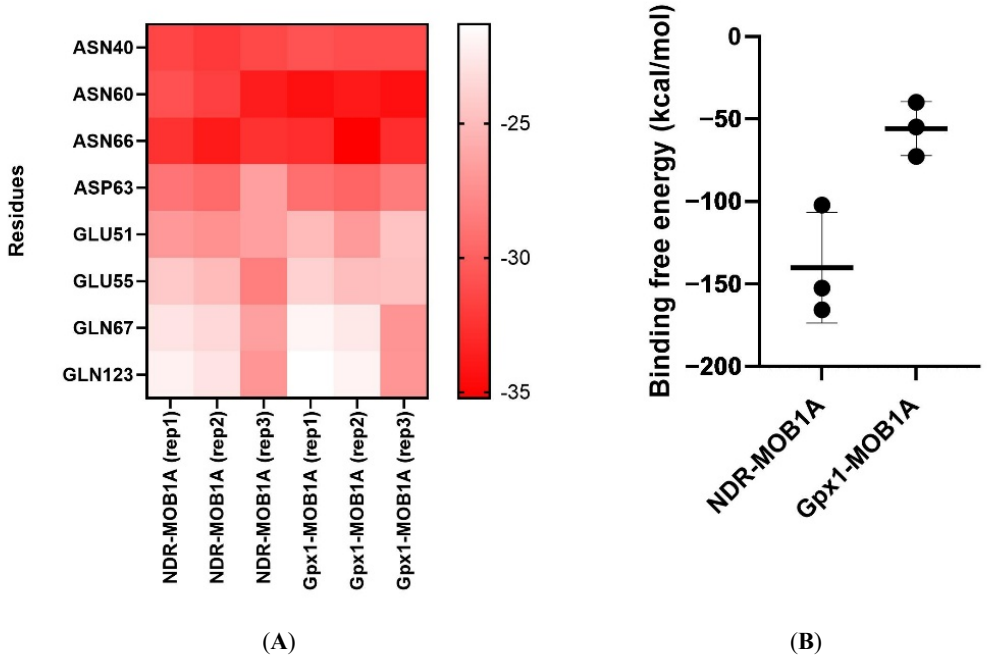

(**A**) (**B**)

Figure 4. Binding interaction analysis of NDR–MOB1A and TmGpx1–MOB1A complexes. (**A**) Heatmap of per-residue binding free energy (ΔG, kcal/mol) of selected MOB1A interface residues from MM/PBSA decomposition across three replicates. Darker colors indicate stronger interactions; crossed cells indicate the absence of a significant contribution. (**B**) Total binding free energy (ΔG, kcal/mol) of each complex. Points represent replicates, and bars indicate mean ± SD. More negative values indicate stronger binding.

The analysis highlights the energetic contribution of individual MOB1A residues to binding with either NDR or TmGpx1. Common hotspots were identified as energetically favorable contributors in both complexes, including ASN40, ASN60, ASN66, ASP63, GLU51, and GLU55. These residues exhibited comparable negative energy contributions across both systems, supporting the structural observation from Figure 1. Both NDR and TmGpx1 proteins interact with overlapping regions on MOB1A. Notably, both proteins rely on the same critical residues, specifically ASN60 and ASN66 (Figure 4A). They emerged as dominant interaction hotspots, showing strong negative energy contributions in both complexes (approximately −30 to −35 kcal/mol stabilization energy), suggesting their central role in stabilizing the interface. Additionally, residues such as ASP63 and GLU51 contributed through electrostatic interactions, likely forming salt bridges or hydrogen bond networks that further stabilize binding. Despite sharing these key touchpoints, the NDR complex displays stronger and more consistent energetic contributions across the entire interface.

In contrast, the TmGpx1 interaction is characterized by reduced energetic optimization and greater variability, which aligns with the lower number of contacts and smaller buried surface area (BSA) observed in structural analyses. This supports the conclusion that while TmGpx1 can engage the canonical MOB1A binding surface, its interaction is comparatively weaker. The NDR–MOB1A complex exhibited a substantially more favorable binding free energy (−140.02 ± 33.52 kcal/mol) compared to the TmGpx1–MOB1A complex (−55.72 ± 16.36 kcal/mol) (Figure 4B). This indicates that the canonical NDR interaction forms a significantly stronger and more energetically stable complex with MOB1A. Although both complexes demonstrated negative binding energies, confirming spontaneous and energetically favorable interactions, the magnitude of binding was markedly reduced in the TmGpx1–MOB1A system. This difference reflects weaker overall intermolecular interactions, consistent with the reduced number of contacts, hydrogen bonds, and smaller buried surface area observed in Figures 2 and 3.

Taken together, these results supported that while TmGpx1 engages the same binding surface on MOB1A, it does so with significantly lower binding affinity compared to the native NDR partner.

4. Discussion

Recent studies have highlighted the frequent targeting of host cellular structures, particularly cytoskeletal and signaling scaffolds, during microbial infection [22]. While much of this understanding originates from plant–pathogen systems, where cytoskeletal remodeling plays a central role in coordinating immune responses and intracellular transport, similar mechanisms are increasingly being recognized in mammalian host–pathogen interactions [23]. In plant models, dynamic reorganization of actin filaments contributes to immune receptor trafficking, reactive oxygen species (ROS) production, and defense signaling [24]. These findings raise an important question in the context of human fungal infections: whether intracellular pathogens such as *T. marneffei* exploit analogous host cellular systems, including signaling scaffolds and structural components, to facilitate survival within macrophages.

In this study, we identified MOB1A as a potential host interactor of TmGpx1 and investigated this interaction through molecular dynamics simulations, using the canonical NDR–MOB1A complex as a reference. MOB1A is a highly conserved scaffold protein in the Hippo signaling pathway, functioning as an activator and adaptor for NDR/LATS kinases [12,13]. Previous structural and biochemical studies have demonstrated that MOB1A contains a negatively charged interaction surface that binds positively charged regions of its kinase partners, enabling proper signal transduction and kinase activation [13]. Therefore, any non-canonical interaction targeting this interface has the potential to interfere with or modulate host signaling processes.

A key observation from our analysis is that the TmGpx1–MOB1A complex shares several overlapping hotspot residues with the NDR–MOB1A complex. These residues, including ASN40, ASN60, ASN66, ASP63, and GLU51, are located within functionally important regions of MOB1A that are known to participate in canonical partner binding. The conservation of these interaction sites suggests that TmGpx1 does not randomly associate with MOB1A but rather targets a biologically relevant binding surface [16]. Similar observations have been reported in bacterial systems, where pathogen-derived proteins exploit conserved host interfaces to modulate signaling pathways. For example, the *Legionella pneumophila* effector kinase LegK7 directly interacts with MOB1A and hijacks the Hippo pathway by phosphorylating MOB1A and promoting downstream signaling alterations [17]. This study demonstrated that pathogen proteins can compete with endogenous partners for MOB1A binding, thereby reprogramming host cellular responses.

Despite this overlap in binding regions, our results indicate that the TmGpx1–MOB1A interaction is structurally and energetically distinct from the canonical NDR–MOB1A complex. Specifically, the TmGpx1 complex exhibited fewer hydrogen bonds, reduced contact numbers, smaller buried surface area, and weaker binding free energy. These differences suggest that TmGpx1 does not function as a direct structural mimic of NDR. Instead, it likely engages MOB1A partially or transiently. This type of interaction is consistent with a regulatory or modulatory role, rather than a fully functional replacement of the endogenous kinase partner. In many host–pathogen systems, such partial interactions are sufficient to disrupt signaling balance or alter protein availability without completely abolishing native interactions.

Although the TmGpx1–MOB1A interaction appears weaker than the canonical NDR–MOB1A complex, weaker or transient interactions can still be biologically meaningful in vivo, particularly in signaling pathways where scaffolding proteins regulate partner availability and complex assembly. We propose that TmGpx1 binding could alter MOB1A configuration and/or compete with endogenous MOB1A partners, thereby shifting Hippo-pathway-associated signaling outputs rather than fully blocking the pathway. Consistent with this concept, the Hippo signaling pathway has been discussed as a contributor to macrophage phenotypic regulation (including M1/M2 polarization states) in the tumor microenvironment and other disease contexts [25]. Thus, even partial engagement of MOB1A by a pathogen-derived protein could plausibly influence macrophage functional state during infection, motivating future experiments to test Hippo pathway readouts and polarization markers in the presence of TmGpx1.

From a biological perspective, this finding is particularly relevant given the intracellular lifestyle of *T. marneffei*. As a pathogen that survives within macrophages, it must withstand oxidative stress and manipulate host defense mechanisms [26]. The glutathione system plays a central role in protecting fungal cells against reactive oxygen species, and glutathione peroxidases such as TmGpx1 are critical components of this defense network [3]. However, increasing evidence suggests that enzymes in this system have additional immunomodulating functions [27]. In this context, our findings are consistent with the hypothesis that TmGpx1 may function as a moonlighting protein. Moonlighting proteins are characterized by their ability to perform multiple, distinct functions depending on cellular context, localization, or interaction partners [10,28]. It is important to emphasize that the moonlighting function of TmGpx1 proposed here is based on computational modeling and yeast two-hybrid screening results. No direct functional assays have yet been performed to demonstrate modulation of host Hippo signaling or

macrophage behavior by TmGpx1. Therefore, this hypothesis remains speculative and requires rigorous experimental validation, such as co-immunoprecipitation, mutagenesis, and functional assays in mammalian macrophages, to confirm the biological relevance of the TmGpx1–MOB1A interaction. Similarly, glutathione peroxidases in other organisms have been reported to exhibit both enzymatic and structural roles, further supporting the possibility of functional diversification. Importantly, proteomic studies have identified glutathione peroxidase among proteins present in EVs derived from *T. marneffei*, indicating that TmGpx1 may be relocalized to its cytosolic environment during infection [7]. EVs-mediated transport could facilitate exposure of TmGpx1 to host proteins such as MOB1A, enabling alternative functions that are not possible within its original intracellular context.

Another notable observation from our simulations is that MOB1A remains structurally stable upon binding to TmGpx1, as indicated by RMSF analysis. This suggests that the interaction does not disrupt the overall fold of MOB1A but may instead influence its interaction dynamics or partner accessibility. Given that MOB1A functions as a signaling scaffold [29], even subtle changes in binding interactions could potentially affect downstream signaling pathways. Previous studies have shown that MOB1A activity is regulated through phosphorylation-dependent conformational changes that control its interaction with kinases [13]. Therefore, binding TmGpx1 to the same or overlapping regions could alter these regulatory mechanisms.

The findings in this study suggested a model in which TmGpx1 interacts with MOB1A at a conserved functional interface but does so in a non-canonical manner that may modulate, rather than replicate, endogenous signaling interactions. This expands the functional landscape of glutathione peroxidase beyond its traditional role in oxidative stress defense and highlights its potential involvement in host–pathogen interaction. Furthermore, it identifies MOB1A as a potential target of fungal proteins, similar to mechanisms observed in bacterial pathogens [17]. However, several limitations should be considered. The interaction identified in this study is based on yeast two-hybrid screening and computational simulations, and experimental validation in mammalian systems is required. Additionally, MM/PBSA calculations provide relative estimates of binding energy and do not fully account for entropic contributions. Future studies should include co-immunoprecipitation assays, mutagenesis of key residues, and functional assays to determine the impact of this interaction on Hippo signaling and macrophage response.

In conclusion, this study provides the first evidence that TmGpx1 may interact with the host signaling protein MOB1A, suggesting that this interaction could represent a novel mechanism of host modulation. By integrating structural, energetic, and comparative analyses, we propose that TmGpx1 functions as a moonlighting protein. It might possess an additional function that extends beyond antioxidant defense to participate in host–pathogen interactions. This work lays the foundation for future studies aimed at understanding how fungal pathogens exploit host signaling networks during infection.

Supplementary Materials

The additional data and information can be downloaded at: https://media.sciltp.com/articles/others/2607301100404212/eMicrobe-26040099-SM.zip. Figure S1: Structural dynamics of protein–protein complexes during molecular dynamics simulations; Figure S2: Backbone RMSD profiles of TmGpx1–MOB1A and NDR–MOB1A complexes during 200 ns molecular dynamics simulations; Table S1: AlphaFold 3 confidence metrics for the predicted TmGpx1–MOB1A and NDR–MOB1A complexes.

Author Contributions

Y.H.H.A. performed the MD simulations; M.P. conceived and supervised the study; Y.H.H.A. generated the figures and tables; Y.H.H.A. and M.P. analyzed data; Y.H.H.A. wrote the original manuscript; M.P. edited and finalized the manuscript. All authors have read and agreed to the published version of the manuscript.

Funding

This research was financially supported by the Faculty of Medicine Research Fund and Thailand Science Research and Innovation (TRSI, Grant no. 4773384). We would like to thank ERAWAN HPC and the Information Technology Service Center (ITSC) of Chiang Mai University for their support with high-performance computing resources.

Institutional Review Board Statement

Not applicable.

Informed Consent Statement

Not applicable.

Data Availability Statement

All data generated or analyzed during this study are included in this published article and its Supplementary Materials.

Conflicts of Interest

The authors declare no conflict of interest.

Use of AI and AI-Assisted Technologies

During the preparation of this work, the authors used AlphaFold 3 through the AlphaFold Server to generate predicted three-dimensional structural models of the TmGpx1–MOB1A and NDR–MOB1A protein complexes for subsequent molecular dynamics simulations. The authors evaluated the generated models using pTM, ipTM, and ranking scores and selected the models used in the study. After using this tool, the authors reviewed and interpreted all outputs and take full responsibility for the content of the published article.

References

1. Brown, L.; Andrianopoulos, A.; Woo, P.C.Y.; et al. The dimorphic fungus *Talaromyces marneffei*: An opportunistic killer in Southeast Asia. *PLoS Pathog.* **2025**, *21*, e1013444. https://doi.org/10.1371/journal.ppat.1013444.
2. Duong, T.A. Infection due to *Penicillium marneffei*, an emerging pathogen: Review of 155 reported cases. *Clin. Infect. Dis.* **1996**, *23*, 125–130. https://doi.org/10.1093/clinids/23.1.125.
3. Wangsanut, T.; Sukantamala, P.; Pongpom, M. Identification of glutathione metabolic genes from a dimorphic fungus *Talaromyces marneffei* and their gene expression patterns under different environmental conditions. *Sci. Rep.* **2023**, *13*, 13888. https://doi.org/10.1038/s41598-023-40932-w.
4. Pongpom, M.; Vanittanakom, N. Stress adaptation in *Talaromyces marneffei*. *Biomed. Sci. Clin. Med.* **2024**, *55*, 23–30.
5. Li, Y.; Li, H.; Sun, T.; et al. Pathogen-host interaction repertoire at proteome and posttranslational modification levels during fungal infections. *Front. Cell. Infect. Microbiol.* **2021**, 11, 774340. https://doi.org/10.3389/fcimb.2021.774340.
6. Wangsanut, T.; Amsri, A.; Pongpom, M. Antibody screening reveals antigenic proteins involved in *Talaromyces marneffei* and human interaction. *Front. Cell. Infect. Microbiol.* **2023**, *13*, 1118979. https://doi.org/10.3389/fcimb.2023.1118979.
7. Pruksaphon, K.; Amsri, A.; Thammasit, P.; et al. Extracellular vesicles derived from *Talaromyces marneffei* contain immunogenic compounds and modulate THP-1 macrophage responses. *Front. Immunol.* **2023**, *14*, 1192326. https://doi.org/10.3389/fimmu.2023.1192326.
8. Yang, B.; Wang, J.; Jiang, H.; et al. Extracellular vesicles derived from *Talaromyces marneffei* yeasts mediate inflammatory response in macrophage cells by bioactive protein components. *Front. Microbiol.* **2021**, 11, 603183. https://doi.org/10.3389/fmicb.2020.603183.
9. Coschigano, P.W.; Magasanik, B. The URE2 gene product of *Saccharomyces cerevisiae* plays an important role in the cellular response to the nitrogen source and has homology to glutathione s-transferases. *Mol. Cell. Biol.* **1991**, *11*, 822–832. https://doi.org/10.1128/mcb.11.2.822-832.1991.
10. Curtis, N.J.; Patel, K.J.; Rizwan, A.; et al. Moonlighting proteins: Diverse functions found in fungi. *J. Fungi* **2023**, *9*, 1107.
11. Wangsanut, T.; Aung, Y.H.H.; Oo, Y.H.H.; et al. Glutathione peroxidase from *Talaromyces marneffei* interacts with host cytoskeletal proteins: Insights from yeast two-hybrid and molecular dynamics simulations. *Int. J. Mol. Sci.* **2026**, *27*, 4259.
12. Stavridi, E.S.; Harris, K.G.; Huyen, Y.; et al. Crystal structure of a human Mob1 protein: Toward understanding Mob-regulated cell cycle pathways. *Structure* **2003**, *11*, 1163–1170. https://doi.org/10.1016/s0969-2126(03)00182-5.
13. Bichsel, S.J.; Tamaskovic, R.; Stegert, M.R.; et al. Mechanism of activation of NDR (Nuclear Dbf2-related) protein kinase by the hMOB1 protein. *J. Biol. Chem.* **2004**, *279*, 35228–35235. https://doi.org/10.1074/jbc.M404542200.
14. Tamaskovic, R.; Bichsel, S.J.; Hemmings, B.A. NDR family of AGC kinases--essential regulators of the cell cycle and morphogenesis. *FEBS Lett.* **2003**, *546*, 73–80. https://doi.org/10.1016/s0014-5793(03)00474-5.
15. Hergovich, A.; Stegert, M.R.; Schmitz, D.; et al. NDR kinases regulate essential cell processes from yeast to humans. *Nat. Rev. Mol. Cell Biol.* **2006**, *7*, 253–264. https://doi.org/10.1038/nrm1891.
16. Gu, J.; Marjanovic, J.; Tomic-Canic, M.; et al. NDR1/2 kinases regulate cell polarization and cell motility through Cdc42 GTPase and Pard3 signaling in mammalian cells. *bioRxiv* **2025**. https://doi.org/10.1101/2025.10.30.685405.

17. Lee, P.-C.; Beyrakhova, K.; Xu, C.; et al. The *Legionella* kinase LegK7 exploits the Hippo pathway scaffold protein MOB1A for allostery and substrate phosphorylation. *Proc. Natl. Acad. Sci. USA* **2020**, *117*, 14433–14443. https://doi.org/10.1073/pnas.2000497117.
18. Abramson, J.; Adler, J.; Dunger, J.; et al. Accurate structure prediction of biomolecular interactions with AlphaFold 3. *Nature* **2024**, *630*, 493–500. https://doi.org/10.1038/s41586-024-07487-w.
19. Astuti, A.D.; Refianti, R.; Mutiara, A. Molecular dynamics simulation on protein using GROMACS. *Int. J. Comput. Sci. Inf. Secur.* **2011**, *9*, 16–20.
20. Wangsanut, T.; Khamto, N.; Pongpom, M. Molecular dynamics simulation to explore functional regions involving Pho4 interaction with co-activator and PHO5 promoter. *eMicrobe* **2025**, *1*, 5. https://doi.org/10.53941/emicrobe.2025.100005.
21. Valdés-Tresanco, M.S.; Valdés-Tresanco, M.E.; Valiente, P.A.; et al. gmx_MMPBSA: A new tool to perform end-state free energy calculations with GROMACS. *J. Chem. Theory Comput.* **2021**, *17*, 6281–6291. https://doi.org/10.1021/acs.jctc.1c00645.
22. Song, M.S.; Lee, D.-K.; Lee, C.-Y.; et al. Host subcellular organelles: Targets of viral manipulation. *Int. J. Mol. Sci.* **2024**, *25*, 1638.
23. Lim, Y.; Cho, Y.B.; Seo, Y.J. Emerging roles of cytoskeletal transport and scaffold systems in human viral propagation. *Anim. Cells Syst.* **2024**, *28*, 506–518. https://doi.org/10.1080/19768354.2024.2418332.
24. Lu, Y.; Zhang, Y.; Lian, N.; et al. Membrane dynamics regulated by cytoskeleton in plant immunity. *Int. J. Mol. Sci.* **2023**, *24*, 6059. https://doi.org/10.3390/ijms24076059.
25. Liu, Y.; An, Y.; Li, G.; et al. Regulatory mechanism of macrophage polarization based on Hippo pathway. *Front. Immunol.* **2023**, *14*, 1279591. https://doi.org/10.3389/fimmu.2023.1279591.
26. Wangsanut, T.; Pongpom, M. The role of the glutathione system in stress adaptation, morphogenesis and virulence of pathogenic fungi. *Int. J. Mol. Sci.* **2022**, *23*, 10645. https://doi.org/10.3390/ijms231810645.
27. Manna, O.M.; Caruso Bavisotto, C.; Gratie, M.I.; et al. The role of *Helicobacter pylori* heat shock proteins in gastric diseases' pathogenesis. *Int. J. Mol. Sci.* **2025**, *26*, 5065. https://doi.org/10.3390/ijms26115065.
28. Lau, S.K.; Tse, H.; Chan, J.S.; et al. Proteome profiling of the dimorphic fungus *Penicillium marneffei* extracellular proteins and identification of glyceraldehyde-3-phosphate dehydrogenase as an important adhesion factor for conidial attachment. *FEBS J.* **2013**, *280*, 6613–6626. https://doi.org/10.1111/febs.12566.
29. Meng, Z.; Moroishi, T.; Guan, K.L. Mechanisms of Hippo pathway regulation. *Genes Dev.* **2016**, *30*, 1–17. https://doi.org/10.1101/gad.274027.115.